Analyst

PAPER

View Article Online
View Journal

Cite this: DOI: 10.1039/c9an01485c

Label-free detection of nosocomial bacteria using a nanophotonic interferometric biosensor†

Jesús Maldonado, [a] M.-Carmen Estévez, *[a] Adrián Fernández-Gavela, [a] Juan José González-López, [b] Ana Belén González-Guerrero [a] and Laura M. Lechuga [a]

Received 3rd August 2019,
Accepted 25th October 2019

DOI: 10.1039/c9an01485c

rsc.li/analyst

Nosocomial infections are a major concern at the worldwide level. Early and accurate identification of nosocomial pathogens is crucial to provide timely and adequate treatment. A prompt response also prevents the progression of the infection to life-threatening conditions, such as septicemia or generalized bloodstream infection. We have implemented two highly sensitive methodologies using an ultrasensitive photonic biosensor based on a bimodal waveguide interferometer (BiMW) for the fast detection of *Pseudomonas aeruginosa* and methicillin-resistant *Staphylococcus aureus* (MRSA), two of the most prevalent bacteria associated with nosocomial infections. For that, we have developed a biofunctionalization strategy based on the use of a PEGylated silane (silane-PEG-COOH) which provides a highly resistant and bacteria-repelling surface, which is crucial to specifically detect each bacterium. Two different biosensor assays have been set under standard buffer conditions: one based on a specific direct immunoassay employing polyclonal antibodies for the detection of *P. aeruginosa* and another one employing aptamers for the direct detection of MRSA. The biosensor immunoassay for *P. aeruginosa* is fast (it only takes 12 min) and specific and has experimentally detected concentrations down to 800 cfu mL^{-1} (cfu: colony forming unit). The second one relies on the use of an aptamer that specifically detects penicillin-binding protein 2a (PBP2a), a protein only expressed in the MRSA mutant, providing a photonic biosensor with the ability to identify the resistant pathogen MRSA and differentiate it from methicillin-susceptible *S. aureus* (MSSA). Direct, label-free, and selective detection of whole MRSA bacteria has been achieved, making possible the direct detection of also 800 cfu mL^{-1}. According to the signal-to-noise (S/N) ratio of the device, a theoretical limit of detection (LOD) of around 49 and 29 cfu mL^{-1} was estimated for *P. aeruginosa* and *MRSA*, respectively. Both results obtained under standard conditions reveal the great potential this interferometric biosensor device has as a versatile and specific tool for bacterial detection and quantification, providing a rapid method for the identification of nosocomial pathogens within the clinical requirements of sensitivity for the diagnosis of infections.

Introduction

Nosocomial infections (infections acquired in the hospital or primary care centers) and the emergence of antibiotic resistant bacteria are major health care issues. Habitually, 1 out of 25 patients in hospitals become infected and as many as 1 in 9 die as a consequence of the acquired infection.[1,2] *Pseudomonas aeruginosa* contributes to 11% of all nosocomial infections, resulting in high mortality and morbidity rates. It is a main causative pathogen of surgical and wound infections, urinary tract infections (UTIs), cystic fibrosis, and bacteremia, with the kidneys, urinary tract, and upper respiratory tract as preferred sites of colonization.[3–5] Methicillin-resistant *Staphylococcus aureus* (MRSA) is a leading pathogen associated with serious hospital diseases.[6–9] MRSA is especially alarming given its multidrug resistance pattern to β-lactam antibiotics. It causes a range of illnesses, from skin and wound infections

[a]*Nanobiosensors and Bioanalytical Applications Group, Catalan Institute of Nanoscience and Nanotechnology (ICN2), CSIC, CIBER-BBN, and BIST, Campus UAB, 08193 Bellaterra, Barcelona, Spain. E-mail: mcarmen.estevez@icn2.cat*

[b]*Department of Clinical Microbiology, Hospital Universitari Vall d'Hebron, Vall d'Hebron Institut de Recerca (VHIR), Universitat Autònoma de Barcelona, 08035 Barcelona, Spain*

†Electronic supplementary information (ESI) available. See DOI: 10.1039/c9an01485c

to pneumonia and bloodstream infections that can result in sepsis and death. MRSA has recently been found to be the main cause of healthcare associated infections (HAI) and in 2014 caused 72 444 invasive infections leading to 13% mortality.[10,11]

Moreover, an early detection of the causative pathogens of nosocomial infections is crucial for prescribing an effective treatment before the disease progresses.[12] A rapid identification of the infective pathogen will greatly help in the selection of the most adequate antimicrobial treatment, limiting broad-spectrum antibiotic therapy and reducing morbidity and mortality. Current methods for bacteria detection in the laboratory involve culture incubation, which takes 2–4 days to complete. Molecular techniques based on PCR detect different nosocomial pathogens in an effective and specific way.[13] However, these techniques also require long and laborious protocols, which can take several hours, and involve trained personnel and specialized equipment. Thus, there is a need for new analytical technologies capable of performing pathogen identification, detection and quantification with high sensitivity, specificity and speed, which circumvent the use of any additional labels and require minimal sample volume and processing.

Several biosensors have been previously employed to detect bacteria, such as surface plasmon resonance (SPR), demonstrating in some cases adequate limits of detection. However, most of these SPR assays do not offer a direct detection of the whole microorganism and rather rely on DNA bacterial extraction and identification,[14] or require the use of nanoparticles and enzymes to amplify the sensor signal.[15] A silicon photonic ring resonator has also been reported as a label-free biosensor for bacterial detection but shows a high limit of detection (10^5 cfu mL^{-1}) due to the lack of an optimized biofunctionalization process.[16] Electrochemical[17–20] and impedimetric biosensors[21] have also been employed for nosocomial pathogen detection, showing good performance and limits of detection (LODs). However, these approaches also need to amplify the signal with enzymes and/or nanoparticles.

The development of biosensors for whole bacteria detection is challenging because bacteria tend to adhere to surfaces. The properties of the sensor surface (*i.e.* charge and hydrophobicity) and the presence of many different antigens on the bacterial surface can easily lead to non-specific interactions with the sensor surface.[22] These interactions can affect the overall signal (*i.e.* resulting in false positive or altered quantifications) and must therefore be minimized as much as possible. Introducing polyethylene glycol (PEG) molecules to cover the surface is a good option as their chemical structure confers high flexibility, hydrophilicity and biocompatibility. Surface modification with PEG to generate bacteria-repelling surfaces has attracted increasing attention[23–26] and grafted PEG coatings have been employed to prevent biofouling by bacteria and cells on different sensor surfaces. However, coating protocols involved complex procedures, such as inert conditions, toxic solvents (*e.g.* benzene and toluene), and intense shaking, and take a long time (>24 h).[27,28] Thus, the generation of a biointerface with the capability of preventing non-specific adhesion by a straightforward method compatible with direct immobilization would be extremely useful in the biosensor field.

Based on this, we have combined a highly sensitive optical biosensor with surface biofunctionalization for the rapid, label-free and specific detection of nosocomial bacteria. In particular, we have employed a photonic biosensor based on bimodal interferometric waveguides (BiMWs), whose sensitivity stands as one of the highest reported in the literature for label-free detection.[29] The working principle of a BiMW biosensor is based on the interferometric design using a single straight waveguide (see Fig. 1). The BiMW sensor has a first waveguide zone exhibiting a single-mode behavior, where only the fundamental mode is propagating. After some distance, the core thickness of the waveguide is increased, acting as a modal splitter and supporting two light modes: the fundamental and the first order mode. Both modes keep travelling through the sensing region of the bimodal device to the output of the waveguide. Both modes have different penetrations of their evanescent fields into the medium and therefore they have different sensitivities to any refractive index change at the sensor surface.[30] Both modes produce an interference pattern at the exit of the waveguide, which is related to the changes induced by any interaction event happening on the sensor surface. This is due to the fact that both modes are differently affected through the evanescent fields which induces a phase variation ($\Delta\Phi$) in the light output. In order to perform the experiments, a sensing window is opened along the bimodal section of the waveguide by removing the top-cladding, allowing the evanescent wave of both modes to be in contact with the biomolecules. This sensing configuration provides an excellent sensitivity with a resolution (minimum detectable change of refractive index) of only 10^{-8} RIU.[29,31]

The BiMW biosensor device has been successfully employed for the rapid detection of *Escherichia coli* and *Bacillus cereus.*[32] We have now modified the silanization protocol to improve even more the surface-repelling properties of the biosensor surface and its usefulness has been demonstrated with the capture and detection of two highly prevalent nosocomial bacteria in a label-free way. Specifically, we have (i) employed a silanization protocol, which involves the formation of a silane-PEG-COOH layer that avoids non-specific bacterial adsorptions on the sensor surface; (ii) developed a BiMW-based immunoassay for *P. aeruginosa* detection; and (iii) developed a detection assay for the specific detection of MRSA based on the use of an aptamer which solely recognizes PBP2a protein, not present in methicillin-susceptible *S. aureus* (MSSA).

The capability of the BiMW biosensor allowed the rapid detection (≤20 min) of whole bacteria at low concentrations (8×10^2 cfu mL^{-1}), estimating a theoretical LOD between 29 and 50 cfu mL^{-1}, without the need for additional amplification steps or sample pretreatment. Our approach exemplifies a proof of concept of a promising alternative for simple, direct, rapid, and label-free bacteria detection, which can further be employed in decentralized settings, such as emergency units, where prompt infection detection and bacterial identification are crucial.

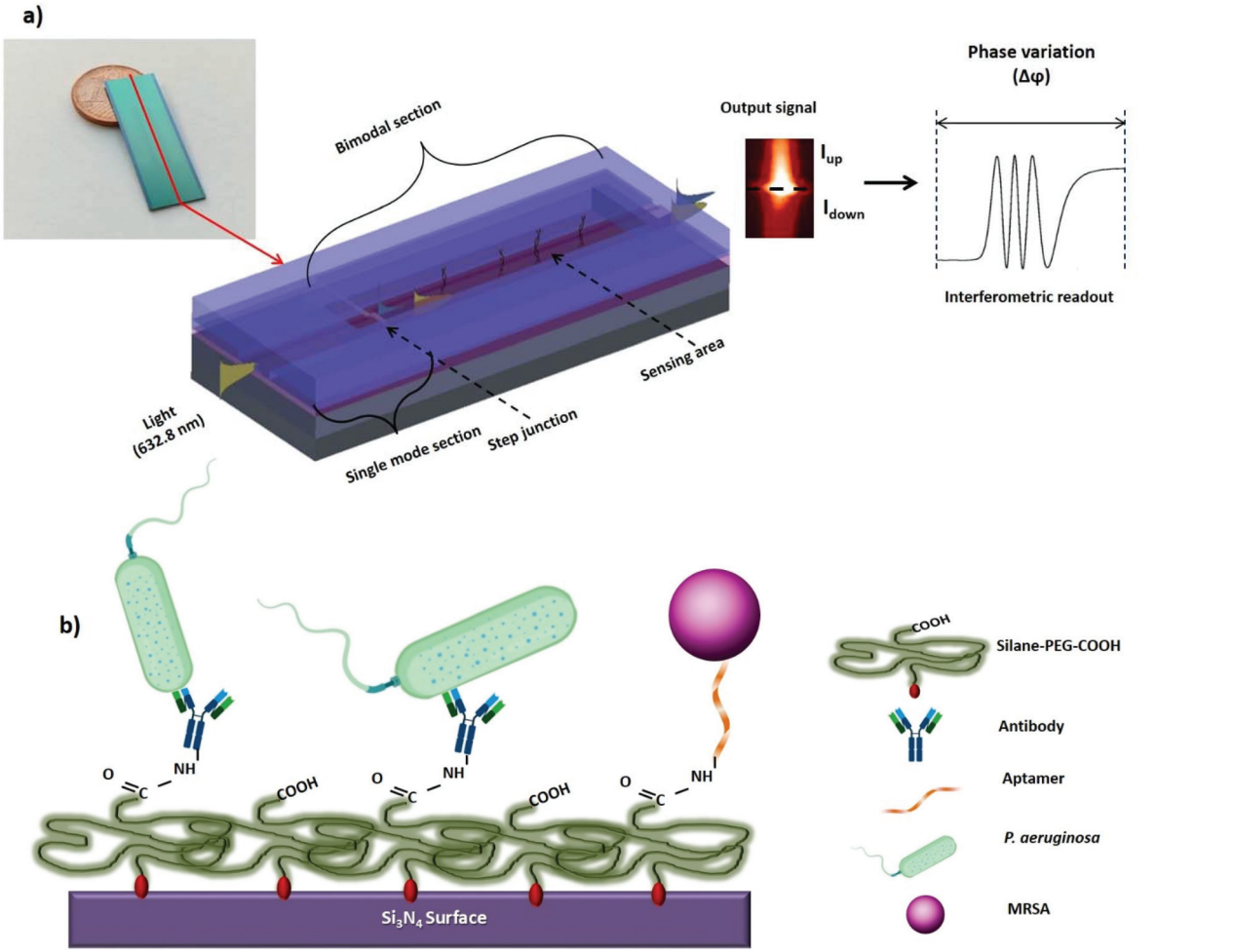

Fig. 1 (a) Scheme of the BiMW device. General view of the main components and the sensing principle. The inset image shows a picture of a BiMW chip containing 20 sensors. (b) Schematic representation of the biofunctionalization strategy: the Si_3N_4 sensor surface is modified with silane-PEG-COOH, and specific bacteria receptors (antibodies or aptamers) are covalently immobilized through the COOH group.

Materials and methods

Chemical and biological reagents

Triethoxysilane polyethylene glycol carboxylic acid (600 Da) (Silane-PEG-COOH) was purchased from Nanocs (USA). Solvents for the sensor cleaning process (dry toluene, acetone, ethanol, hydrochloric acid (HCl, 35–38%), and methanol) were supplied by Panreac (Spain). 1-Ethyl-3(3-dimethylaminopropyl) carbodiimide hydrochloride (EDC), *N*-hydroxysulfosuccinimide (sulfo-NHS), the reagents for glutaraldehyde buffer preparation, and $MgCl_2$ (1 mM) were purchased from Sigma-Aldrich (Spain). The buffers employed are the following: PBS (10 mM phosphates, 2.9 mM KCl, 137 mM NaCl, pH 7.4); PBST (PBS with 0.005% Tween 20); MES (0.1 M, 0.5 M NaCl, pH 5.5); and HEPES (10 mM, pH 7.4); SU-8 2025 and polydimethylsiloxane (PDMS) polymers used for the flow cell fabrication were purchased from Microchem (USA) and Sylgard® (USA), respectively.

Polyclonal anti-*Pseudomonas* antibody was purchased from Abcam® (Spain). All bacterial strains were provided by the Vall d'Hebron Hospital (Barcelona, Spain). The bacteria were streaked onto Luria broth (LB) and incubated overnight at 37 °C. Purification of bacteria was carried out by centrifugation at 3000 rpm for 15 min at 4 °C. Bacteria were then suspended in PBST (*P. aeruginosa* and *E. coli*) or PBS (MRSA and MSSA). Bacteria concentrations were directly calculated with a UV/VIS spectrophotometer (Nanophotometer™ from Implen, Germany) by measuring the optical density (OD) at 600 nm every time a new culture sample was used. Subsequent dilutions were made for each experiment to cover the range of analysis. The *MRSA* aptamer with an amino modification at the 3′ end (5′-Aptamer-NH_2-3′) and recombinant *S. aureus* PBP2a protein were purchased from Base Pair Technologies (USA). The dry aptamer was suspended in PBS buffer at a final concentration of 100 μM. Once the aptamer is dissolved in the buffer, it must be heated to 90 °C for 2 min and then cooled down to room temperature before use.

BiMW sensor and experimental set-up

The BiMW sensors are designed and fabricated at the wafer level using standard microelectronic technology in clean room

facilities as previously described.[33] Each wafer contains 12 sensing chips, and each chip includes an array of 20 bimodal waveguide interferometric sensors of 30 mm length with a pitch of 250 μm between them. Each sensor consists of a silicon nitride (Si_3N_4) waveguide covered with a silicon oxide (SiO_2) layer used as cladding. These materials have been selected due to their high refractive index contrast. The thickness of the core layer in the single-mode section must be 150 nm to obtain the best yield of the light at the output of the devices. The rib depth value is of a few nanometers (1–3 nm) and the values for the width are around 2.5–3 μm to obtain a single mode behaviour in the *y* coordinate.

A scheme of the employed experimental set-up is shown in the ESI (Fig. S1†). The experimental set-up includes the following modules: a laser, optical components, a microfluidic delivery system, a temperature controller, a photodetector, and electronics and data acquisition. A He–Ne laser (λ = 632.8 nm, TE polarization) is employed as the light source, a 40× microscope objective and a beam expander are employed for light in-coupling and a two-section Si photodiode is employed for out-coupling detection. The intrinsic sensitivity of the BiMW device to external temperature fluctuations was compensated by incorporating a Peltier element behind the sensor chip and a temperature controller, providing temperature stabilization with an accuracy of 0.01 degrees. The flow delivery system includes a syringe pump for the continuous delivery of the buffer and an injection valve connected to a loop of 150 μL for injecting the samples. The interferometric sensor signal (%) is obtained directly from the intensity received in the two-section photodetector during the real time measurements[32] This can be expressed as phase variation ($\Delta\Phi$) considering that a complete interferometric oscillation or fringe corresponds to a 2π rad phase variation. For clearer presentation, calibration curves are represented as $\Delta\Phi$ *vs*. concentration. The data acquisition and analysis included a computer with a data acquisition card, home-made LabVIEW software, and Origin 8.0 software (Originlab, Northampton, MA).

For biosensing evaluation in continuous flow and in order to perform the analysis of aqueous samples, it was necessary to incorporate a microfluidic cell and a flow delivery system. The microfluidic cell was fabricated using PDMS polymer, building a microfluidic cell with eight channels with a pitch of 250 μm between them. Each microchannel has a length of 18 mm, a height of 50 μm and a width of 100 μm, which covers the sensing window of each sensor. The alignment of the microfluidic system over the bimodal waveguide sensor was performed using a home-made aligner, which comprises three 3-axis micromanipulators and a vacuum pump. In order to obtain a continuous flow, the microfluidic cell was connected to the fluidic system described in the previous section. The volume flow rate was modified according to the bioassay requirements, oscillating between 5 and 30 μL min^{-1}.

Sensor chip cleaning and chemical activation

The BiMW sensor chips were sonicated in acetone, ethanol, Milli-Q water and 1 : 1 methanol/HCl solution in order to remove organic contamination. Then they were rinsed with Milli-Q water and dried with a N_2 stream. An oxidation step to reveal enough oxide groups on the sensor surface was carried out by placing the sensor chips in a UV/O_3 cleaner (BioForce Nanosciences, USA) for 1 h, followed by their exposure to 10% nitric acid solution at 75 °C for 25 min. After rinsing with Milli-Q water, the sensor chips were incubated with 25 mg mL^{-1} silane-PEG-COOH solution in ethanol/water 95 : 5 (v/v) for 2 h at 4 °C. Then the sensor chips were rinsed with ethanol and water and dried with a N_2 stream. A final curing step was performed by introducing the sensor chips into a glass bottle and inside a conventional autoclave for 90 min at 120 °C at a pressure of 1.5 bars.

Antibody biofunctionalization and assay development

Antibody immobilization was performed *in situ* (*i.e.* by mounting the silanized sensor chip with the flow cell, placing it in the optical setup and flowing the different solutions). Anti-*Pseudomonas* antibodies were immobilized on the sensor surface through covalent binding to the carboxyl groups introduced on the sensor surface during the silanization process. Carboxyl groups were first activated by flowing a solution of 0.2 M EDC/0.05 M sulfo-NHS in MES buffer. Next, a solution of anti-*Pseudomonas* (50 μg mL^{-1} in PBS) was injected over the freshly activated sensor surface at a flow rate of 10 μL min^{-1}. After immobilization, Milli-Q water was switched to PBST as a running buffer, which was circulated over the sensor surface at a constant flow of 20 μL min^{-1}. Bacterial samples (between 8×10^2 and 1×10^7 cfu mL^{-1} in PBST) were loaded into a 150 μL loop and flowed over the sensor surface with a flow rate of 20 μL min^{-1}. 100 mM HCl solution (injected at 30 μL min^{-1}) was used as a regeneration buffer to break the bacteria/antibody interaction. Calibration curves were obtained for each bacterium after performing triplicate measurements of different samples of known concentration. The theoretical LOD was estimated as the concentration corresponding to the minimum measurable signal, set as three times the standard deviation (SD) of the baseline of the sensor signal.

Aptamer biofunctionalization and assay development

Aptamer immobilization was carried out using an *ex situ* protocol (*i.e.* outside the optical setup following successive incubation/washing steps). In this case, the sensor surface was activated with a solution of 0.4 M EDC/0.1 M sulfo-NHS in MES buffer for 3 h. After rinsing with water, an aptamer solution (2 μM in PBS containing 1 mM $MgCl_2$) was incubated over the sensor surface overnight at room temperature. Finally, the sensor chip was washed with PBS and water, dried with a N_2 stream and mounted on the experimental setup. PBS buffer was set as a running buffer for MRSA detection. All the bacterial samples (ranging from 8×10^2 to 1.6×10^7 cfu mL^{-1}) were loaded in a 150 μL loop and flowed over the sensor surface at a flow rate of 20 μL min^{-1}. After each measurement, HCl (25 mM injected for 60 s at 20 μL min^{-1}) was flowed to dissociate the interaction, regenerate the aptamer and reuse the aptasensor.

SEM analysis

The images of bacterial adhesion to the sensor surface were examined by using a 400L field-emission scanning microscope (FE-SEM; FEI Magellan) operated at an acceleration voltage of 2 kV and with a working distance of 4.5 mm. A Quanta 650F Scanning Electron Microscope (Field Emission Inc., USA), operated at 2 kV, was used to assess the selectivity of the aptamer for the detection of MRSA, confirming the binding of whole MRSA on the aptamer-modified sensor surface. All bacteria were first suspended in PBST buffer. Si_3N_4 surfaces without and with silane-PEG-COOH and biofunctionalized with the aptamer were placed in a solution of 10^7 cfu mL^{-1} of each bacterium for 1 h, and then PBST buffer was replaced by a fixation buffer (glutaraldehyde 5% in HEPES buffer) and incubated for another hour. The Si_3N_4 surfaces were washed with PBST and dried with a N_2 stream before examination by SEM.

Results and discussion

Analysis of bacterial adhesion onto the silicon nitride sensor surface

A key point in the development of a surface refractive index based biosensor is to completely avoid unspecific adsorptions. In general, any adsorbed mass on the surface produces a refractive index change and, therefore, results in altered sensor values that affect accurate quantification. In this context, bacteria are especially complex targets since they are prone to adsorb on any type of surface, giving rise to unspecific responses in biosensors, which cannot be distinguishable from the specific ones. The design of a surface that minimizes other bacteria adhesions, that only allows the interaction of the target bacteria with their specific bioreceptor but not with the sensor surface, and that ideally avoids additional blocking steps is mandatory for the achievement of competitive and high performance bacterial biosensors. PEG is known to decrease the interaction between silicon surfaces and biomolecules because of its steric stabilization forces and chain mobility.[34] Therefore, we used a silane containing short chain PEG (MW = 600 Da) with a carboxylic group at the other end, in such a way that it provided a reactive group to be further coupled to bioreceptors. A simple silanization protocol was followed based on the incubation of the biMW chip with the silane-PEG-COOH, followed by an autoclaving process. This strategy resulted in a stable and dense covalently bound PEGylated layer. The PEGylated layer was evaluated by X-ray photoelectron spectroscopy (XPS) (see the ESI† for detailed information). The non-specific adsorptions of different bacteria on Si_3N_4 surfaces coated with the silane-PEG-COOH were first evaluated using *S. aureus*, as a representative model of Gram-positive bacteria and *E. coli* and *P. aeruginosa* as representatives of Gram-negative bacteria. They were selected since they are three of the most common pathogens identified in nosocomial infections. As can be seen in Fig. 2(top), significant non-specific adsorptions of bacteria over untreated Si_3N_4 surfaces were clearly observed, being particularly high for *S. aureus* (Gram-positive) in comparison with *E. coli* and

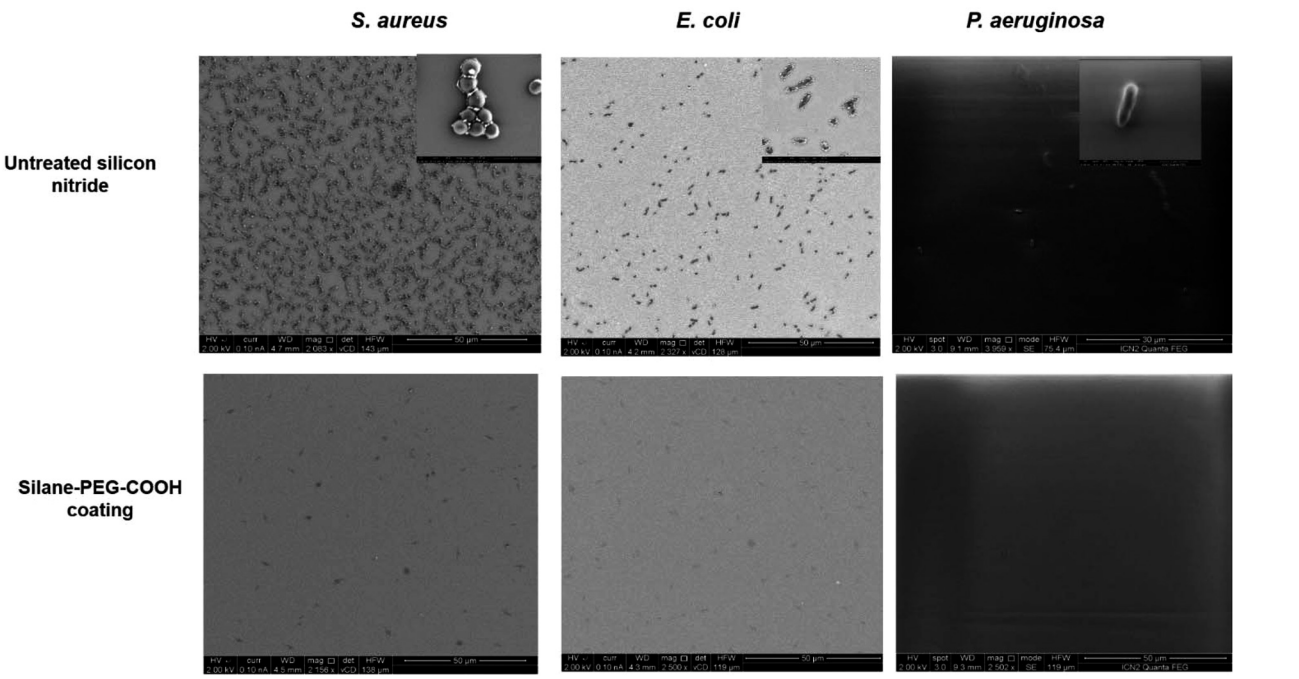

Fig. 2 SEM images of the bacterial adhesion on untreated Si_3N_4 sensor surfaces (top) and on a sensor surface treated with PEG-silane-COOH (bottom). Scale bars of inset images (top) are 2, 5, and 1 μm, respectively.

mainly with *P. aeruginosa* (Gram-negative), which showed a much lower adhesion. These results also exemplify how different bacteria can behave in terms of adsorption depending on their own surface properties. Even in the case of *P. aeruginosa*, with an apparently low adhesion, the resultant signal of the biosensor could be comparatively high, considering the size of bacteria and the extreme sensitivity level of our device.[29] On the other hand, the SEM images of the silanized surfaces demonstrate that the surface treatment with PEGylated compounds such as the silane-PEG-COOH helps prevent the bacterial adhesion (see Fig. 2, bottom) with all the three bacteria tested. Finally, the ability of the silane-PEG-COOH modified surface to attach biomolecules was then assessed with the immobilization of the antibodies (through the free Lys in their structure) and confirmed using XPS. For this experiment, the silicon nitride surface was cleaned and modified with silane-PEG-COOH, then the carboxyl groups were activated with a solution of EDC/sulfo-NHS, and an antibody solution (50 μg mL^{-1}) was incubated over the silicon nitride surface for 30 min at room temperature. The details of XPS experiments and the comparison of the survey spectra for untreated Si_3N_4, silane-PEG-COOH and sensor surfaces with immobilized antibody are discussed in the ESI and Fig. S1–S4† therein.

Immunoassay for the detection of *Pseudomonas aeruginosa*

The BiMW sensor modified with silane-PEG-COOH was placed in the experimental set-up. Then, the carboxyl groups of the silane-PEG-COOH surface were activated with a solution of EDC/sulfo-NHS. An antibody solution was flowed over the sensor surface and the immobilization was monitored in real-time. The mean immobilization signal of the antibody was 7.5 ± 2 × 2π rad, which represents a high and reproducible antibody coverage due to the covalent attachment (Fig. S5†). Suspensions of *P. aeruginosa* at different concentrations were sequentially flowed through the sensor surface. Representative signals of specific *P. aeruginosa* detection (1.6×10^5 cfu mL^{-1}) and non-specific *E. coli* (1×10^5 cfu mL^{-1}) used as a control are shown in Fig. 3a. These results show a $\Delta\Phi$ of 0.4 × 2π rad for the detection of *P. aeruginosa* and a negligible signal for the *E. coli* sample, respectively, which confirms the specificity of the immunoassay provided by the antibody. Additional *E. coli* samples at different concentrations (from 10^5 to 10^7 cfu mL^{-1}) were also flowed and no signal was observed for any of them, confirming that the signal contribution was coming only from the specific detection of *P. aeruginosa* (see Fig. 3b). The interaction between the antibodies and the captured bacteria can be further interrupted by the injection of 100 mM HCl for 1 min (see the sensorgram in Fig. 3c as a representative binding and regeneration cycle) without altering the sensor surface density of antibodies, as can be seen by the complete recovery of the baseline. Under these conditions, the biosensor was reusable for up to 5 cycles using the same bioreceptor layer before degradation of the antibody layer (*i.e.* the signal corresponding to bacteria binding decreased significantly). A calibration curve was generated after analyzing a wide range of bacterial concentrations. The lowest concentration analyzed was 8×10^2 cfu mL^{-1}, resulting in a $\Delta\Phi$ of 0.074 × 2π rad (see Fig. 3b). Considering the sample volume injected (*i.e.* 150 μL) this corresponds to 120 bacteria detected. Moreover, considering the minimum measurable signal, which was set as three times the standard deviation of the baseline ($8.5 \times 10^{-5} \times 2\pi$ rad), we could estimate a theoretical LOD of 49 cfu mL^{-1}. Nevertheless, even the lowest concentration experimentally measured, 800 cfu mL^{-1}, falls within the cut-off values in infections such as UTIs (*i.e.* between 10^4–

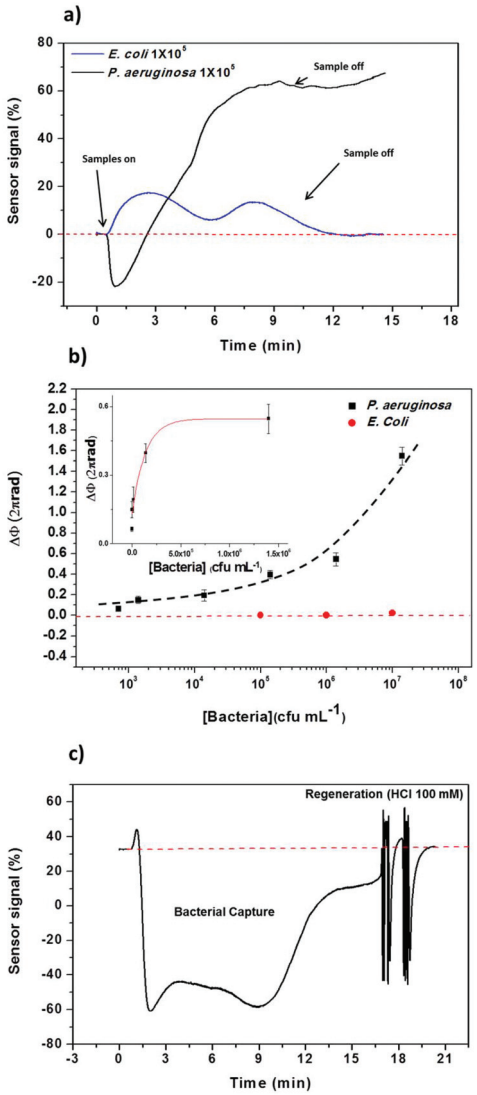

Fig. 3 (a) Real time interferometric signals obtained for *P. aeruginosa* and *E. coli* (negative control). (b) Calibration curve for *P. aeruginosa* (black squares) and for non-specific bacteria *E. coli* (red circles). Inset graph: linear representation with exponential fitting ($y = y_0 + Ae^{-x/t}$) of the *P. aeruginosa* detection. The linear part was fitted to a linear regression ($y = 1.7484 \times 10^{-6}x$, $R^2 = 0.9846$). All data show mean ± SD of triplicate measurements. (c) Real time interferometric signal of *P. aeruginosa* detection (1.6×10^3 cfu mL^{-1}), followed by a regeneration step (the dashed line indicates the baseline).

10^5 cfu mL^{-1})[35] and upper and lower respiratory tract infections (cut-off at 10^3 cfu mL^{-1})[36,37] and could even be suitable for more restrictive cut-offs such as for blood stream infections.[38]

Aptamer-based assay for the detection of MRSA

Detection of PBP2a protein. Methicillin-resistant *S. aureus* emerges after acquiring the *mecA* resistance gene, which encodes PBP2a protein.[39,40] This protein is a unique transpeptidase that catalyzes cell-wall crosslinking and it is not inhibited by β-lactam antibiotics (contrary to what happens with the four *S. aureus* native Penicillin-binding proteins (PBPs)). Therefore, the detection of this distinctive protein, only present in the MRSA strain, is a specific approach to identify these bacteria. Besides antibodies commercially available, a specific aptamer was recently developed that specifically recognizes PBP2b. In order to take advantage of the silane-PEG-COOH chemistry, we decided to modify the aptamer with an amino ($-NH_2$) terminal group and use the same surface chemistry employed with the antibody previously. We first attempted the detection of pure PBP2a protein in order to evaluate the affinity and the integrity of the aptamer after immobilization and its specificity against other interfering proteins. As a negative control, we selected a protein located in the cell wall of *Mycobacterium tuberculosis* (also a Gram-positive bacterium, such as MRSA) as PBP2b in MRSA. The capability of the aptamer to detect PBP2a protein was evaluated at different concentrations (between 50 and 500 ng mL^{-1}); the negative control protein was tested at two concentrations: 500 ng mL^{-1} and 5 μg mL^{-1} (ten times higher than the highest concentration of PBP2b evaluated). Representative signals of the two concentrations of PBP2a and the negative control are shown in Fig. 4a. These signals show a $\Delta\Phi$ of 0.1 × 2π rad for the detection of 100 ng mL^{-1} and 0.3 × 2π rad for the detection of 500 ng mL^{-1} of PBP2a protein, respectively, while the signals for the negative controls are negligible, indicating the excellent specificity of the aptamer. The range of PBP2a concentrations evaluated showed a linear concentration-dependent profile as can be seen in Fig. 4b and c. A calibration curve for the direct detection of PBP2a was generated, reaching an estimated LOD of 3.27 ng mL^{-1} (Fig. 4c).

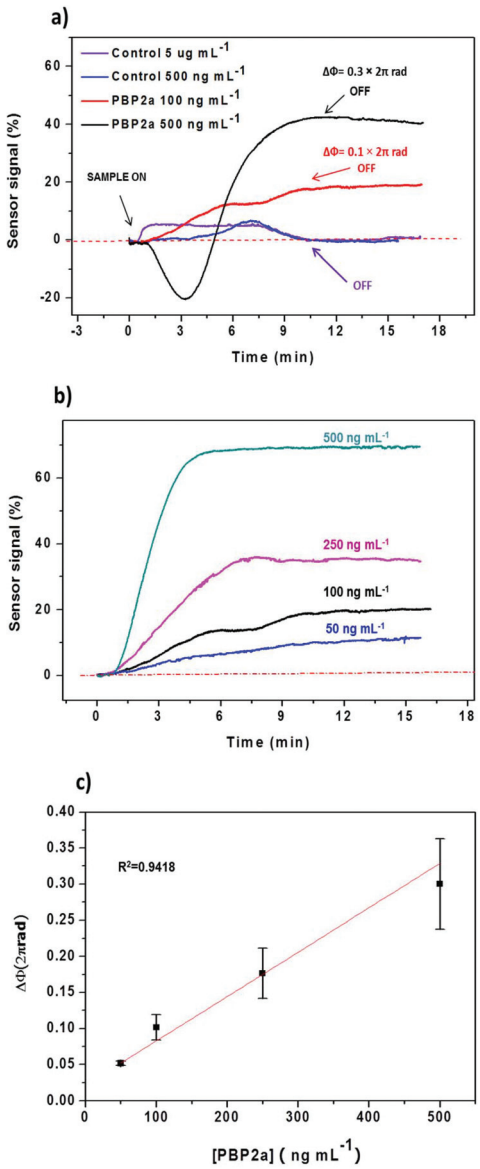

Fig. 4 (a) Real time interferometric signal obtained for the detection of PBP2a protein and for the control protein over the aptamer biofunctionalized sensor. (b) Real time interferometric signals for several PBP2a concentrations over aptamer-modified sensor chips. (c) Calibration curve obtained for PBP2a protein in buffer. All data show mean ± SD of triplicate measurements.

Detection of MRSA bacteria. In order to evaluate the capability of the aptasensor for whole MRSA detection and establish its overall performance, several solutions of MRSA bacteria were prepared in PBS and injected over the aptamer modified sensor surface. MSSA was also analyzed to assess the specificity provided by the aptamer. Representative signals of MRSA (1.6×10^6 cfu mL^{-1}) and MSSA (2×10^6 cfu mL^{-1}) detection are shown in Fig. 5a. These signals show a $\Delta\Phi$ of 0.41 × 2π rad for the detection of MRSA, and no signal for the MSSA sample. We established the regeneration conditions that enable the dissociation of the MRSA-aptamer binding, without affecting the aptamer activity or integrity as can be seen in Fig. 4b; the use of 25 mM HCl for 60 s was enough to disrupt the interaction and remove all the bacteria bound to the aptamer, therefore fully recovering the baseline. Other solutions such as NaOH or NaCl were not able to dissociate the interaction or they affected the conformation of the aptamer, disabling it for further interactions. Under the optimal regeneration conditions, the biosensor could be reused up to 12 cycles before signal decreases (see Fig. S6 in the ESI†). Fig. 5c shows some representative signals of specific MRSA detection at different concentrations. The calibration curve is depicted in Fig. 5d. A $\Delta\Phi$ signal of 0.04 × 2π rad was observed for the lowest concentration injected (8×10^2 cfu mL^{-1}) and increased gradually as the bacterial concentration was also higher. Considering the baseline signal ($8.5 \times 10^{-5} \times 2\pi$ rad), an estimated theoretical LOD of around 29 cfu mL^{-1} was calculated from the linear

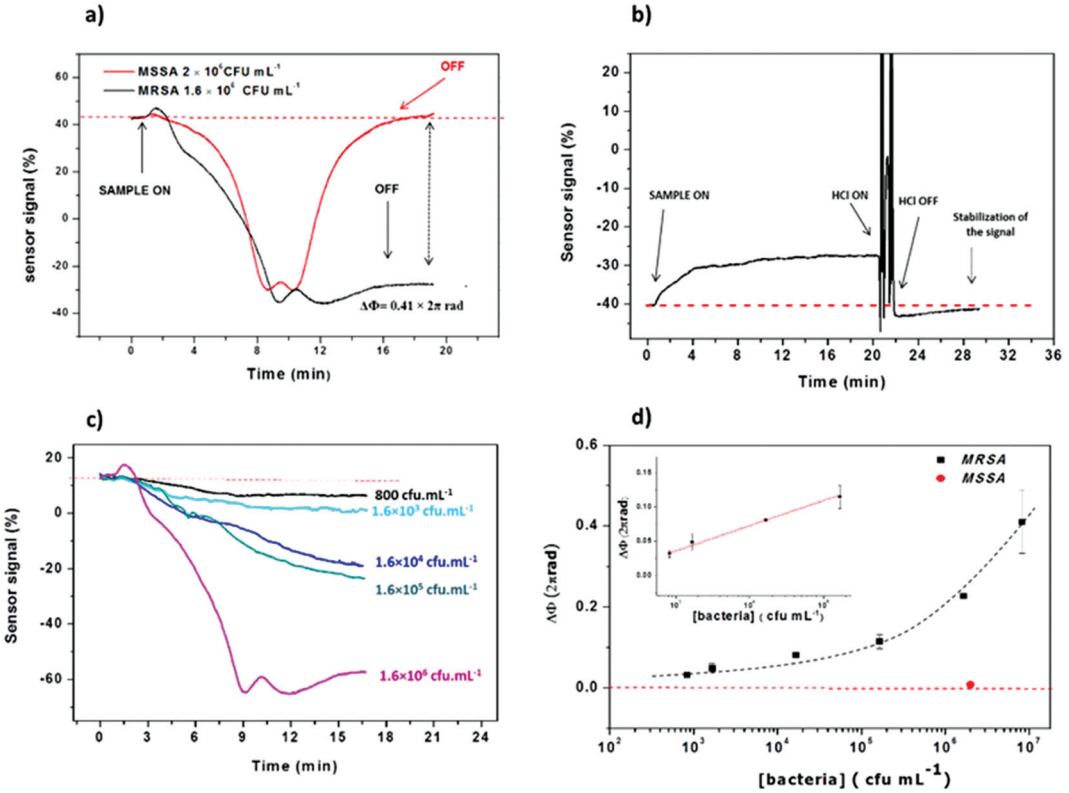

Fig. 5 (a) Real time interferometric signal of MRSA (black line) *versus* MSSA measurement (red line); (b) real time interferometric signals of the MRSA detection, followed by the regeneration step with HCl 25 mM; (c) real time interferometric signals showing the detection of MRSA bacteria at different bacterial concentrations (the red dashed line indicates the baseline). (d) Calibration curve for whole MRSA detection with the BiMW aptasensor. The signal obtained for MSSA at 10^6 cfu mL^{-1} is also shown. The inset graph shows the linear fitting ($y = 2.967 \times 10^{-6}x$, $R^2 = 0.9697$) for the low bacterial concentration range (*i.e.* between 800 and 1.6×10^5 cfu mL^{-1}). All data show mean ± SD of triplicate measurements.

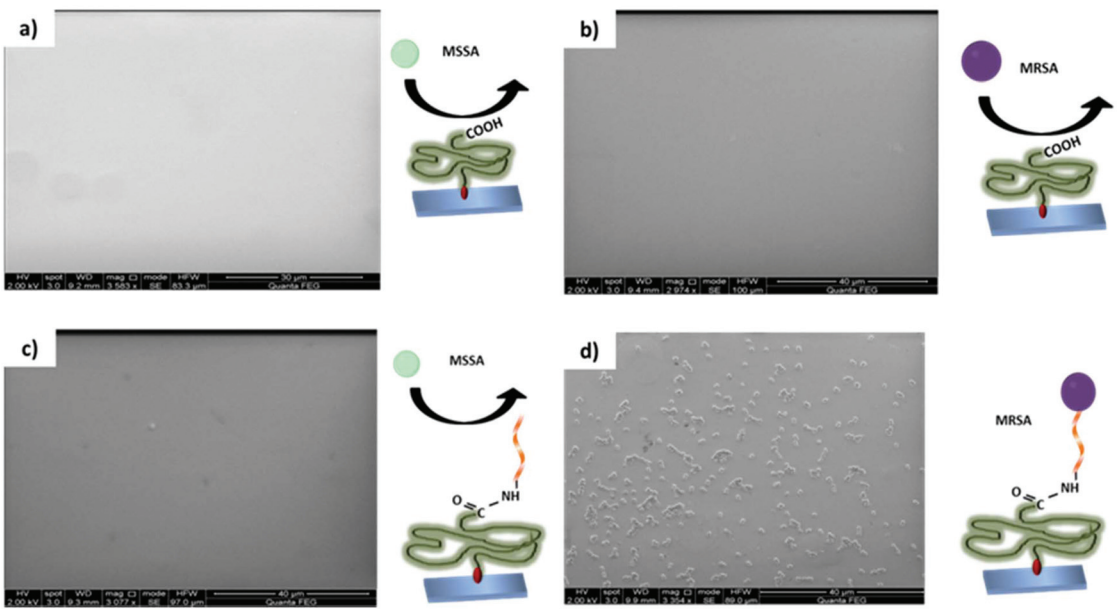

Fig. 6 SEM study for the confirmation of the selectivity and specificity of the MRSA aptamer biofunctionalized Si_3N_4 sensor surfaces. (a) MSSA (10^7 cfu mL^{-1}) on a Si_3N_4 sensor surface modified with only silane-PEG-COOH (*i.e.* no aptamer immobilized); (b) MRSA (10^7 cfu mL^{-1}) on a Si_3N_4 sensor surface modified with only silane-PEG-COOH (*i.e.* no aptamer immobilized); (c) MSSA (10^7 cfu mL^{-1}) on a sensor surface with MRSA aptamer immobilized and (d) MRSA (10^7 cfu mL^{-1}) on a sensor surface with MRSA aptamer immobilized.

fitting for the MRSA detection (inset in Fig. 5d). This level is comparable to the one obtained for *P. aeruginosa* using antibodies, complying also with the current clinical requirements for the detection of nosocomial infections.[41,42]

We performed SEM analysis for additional confirmation of the specificity provided by the employed aptamer and the selectivity generated by the biofunctionalization protocol. For that, we incubated several sensor surfaces with the bacteria. Fig. 6(a) and (b) show sensor surfaces with only the silane-PEG-COOH (*i.e.* no aptamer present), exhibiting a complete lack of non-specific binding of bacteria, both for MRSA and MSSA, which demonstrates the microbial-repelling property of the monolayer, as previously discussed. Additionally, on sensor surfaces with the aptamer already immobilized, we only observed the capture of MRSA (see Fig. 6(d)) whereas MSSA was not captured (see Fig. 6(c)), ratifying the specificity features of this aptamer to solely detect MRSA bacteria and the total discrimination of MSSA.

Conclusions

We have implemented a rapid, label-free, and highly sensitive BiMW biosensor able to identify and quantify nosocomial bacteria. Our strategy is based on the combination of a sensor surface modified with silane-PEG-COOH, which provides an excellent bacteria-repelling coating, and the use of appropriate specific receptors (*i.e.* both antibodies and aptamers). With this biofunctionalization strategy, non-specific bacterial adsorption was successfully eliminated under standard buffer conditions, avoiding extra blocking steps, which can lengthen the process and affect the final sensitivity. The silane-PEG-COOH surface was evaluated using SEM to assess its performance and its bacteria-repelling capabilities and the biofunctionalized surface was additionally characterized with XPS. The subsequent addition of a suitable antibody layer led to a BiMW immunosensor that showed a selective label-free detection of *P. aeruginosa* with an estimated theoretical LOD of 49 cfu mL^{-1}. Moreover, the versatile chemistry provided by the COOH groups in the silanized sensor chips also facilitated the immobilization of an amino-modified aptamer, providing an efficient and highly specific detection of MRSA bacteria at concentrations as low as 800 cfu mL^{-1}, making possible the estimation of a theoretical LOD of 29 cfu mL^{-1} and avoiding any recognition of MSSA. The combination of the high sensitivity of the BiMW sensor with the features of the specific aptamer represents an excellent analytical tool to distinguish between resistant and susceptible *S. aureus* in a direct and rapid way.

The methodology used to generate the bacteria-repelling surface, based on a simple process of autoclave curing of a reactive silane, has proven to be very useful under buffer conditions. Further testing with more complex and challenging fluids (*i.e.* urine or serum, whose composition can include different substances that can affect the sensing performance) must be evaluated. This strategy can be employed as a general methodology for developing stable modified sensor surfaces for other silicon photonic biosensors. Overall, the results obtained demonstrate the competitive potential of the BiMW biosensor technology, in combination with a silane-PEG-COOH interface, to provide a label-free, rapid, stable, selective and specific biosensor device for the identification of nosocomial pathogens. The turnaround analysis time of around 15 min under buffer conditions is significantly shorter than that of, for example, conventional ELISA, even if simple sample pretreatment (*i.e.* centrifugation and resuspension to remove undesired effects of biological fluids) was eventually required. Moreover, our approach could be further translated to a multiplexed configuration by simply addressing the immobilization of different antibodies and aptamers in each individual bimodal waveguide and could be easily integrated in a point-of-care instrument to be deployed in clinical settings, in order to facilitate fast bacterial diagnosis, one of the urgent needs in our healthcare system.

Conflicts of interest

There are no conflicts to declare.

Acknowledgements

The work was supported by CIBER-BBN (Networking Center on Bioengineering, Biomaterials and Nanomedicine) through the Intramural Project ASPIRE. J. Maldonado acknowledges the Mexican National Council for Science and Technology (CONACYT). ICN2 was supported by the Severo Ochoa program from Spanish MINECO (Grant No. SEV-2017-0706).

References

1 K. S. Park, C. H. Huang, K. Lee, Y.-E. Yoo, C. M. Castro, R. Weissleder and H. Lee, *Sci. Adv.*, 2016, **2**(5), e1600300.
2 S. S. Magill, J. R. Edwards, W. Bamberg, Z. G. Beldavs, G. Dumyati, M. A. Kainer, R. Lynfield, M. Maloney, L. McAllister-Hollod, J. Nadle, S. M. Ray, D. L. Thompson, L. E. Wilson and S. K. Fridkin, *N. Engl. J. Med.*, 2014, **370**, 1198–1208.
3 M. Balasoiu, A. T. Balasoiu, R. Manescu, C. Avramescu and O. Ionete, *Curr. Health Sci. J.*, 2014, **40**, 85–92.
4 P. Shukla, R. K. Garg and A. K. Dahiya, *Apollo Med.*, 2016, **13**, 71–73.
5 J. B. Lyczak, C. L. Cannon and G. B. Pier, *Microbes Infect.*, 2000, **2**(9), 1051–1060.
6 S. Stefani, D. R. Chung, J. A. Lindsay, A. W. Friedrich, A. M. Kearns and H. Westh, *Int. J. Antimicrob. Agents*, 2012, **39**, 273–282.
7 X. Lu, D. R. Samuelson, Y. Xu, H. Zhang, S. Wang, B. A. Rasco, J. Xu and M. E. Konkel, *Anal. Chem.*, 2013, **85**, 2320–2327.
8 S. R. Harris, E. J. Feil, M. T. Holden, M. A. Quail, E. K. Nickerson, N. Chantratita, S. Gardete, A. Tavares,

N. Day, J. A. Lindsay, J. D. Edgeworth, H. de Lencastre, J. Parkhill, S. J. Peacock and S. D. Bentley, *Science*, 2010, **327**, 469–474.

9 K. T. Kavanagh, L. E. Calderon and D. M. Sama, *Antimicrob. Resist. Infect. Control*, 2015, **4**, 4.

10 Centers for Disease Control and Prevention. *Active bacterial core surveillance report, emerging infections program network, methicillin resistant Staphylococcus aureus*, 2014.

11 A. Hassoun, P. K. Linden and B. Friedman, *Crit. Care*, 2017, **21**, 211.

12 S. Harbarth, J. Garbino, J. Pugin, J. A. Romand, D. Lew and D. Pittet, *Am. J. Med.*, 2003, **115**, 529–535.

13 K. L. Thong, M. Y. Lai, C. S. Teh and K. H. Chua, *Trop. Biomed.*, 2011, **28**, 21–31.

14 K. Nawattanapaiboon, W. Kiatpathomchai, P. Santanirand, A. Vongsakulyanon, R. Amarit, A. Somboonkaew, B. Sutapun and T. Srikhirin, *Biosens. Bioelectron.*, 2015, **74**, 335–340.

15 F. Melaine, M. Saad, S. Faucher and M. Tabrizian, *Anal. Chem.*, 2017, **89**, 7802–7807.

16 A. Ramachandran, S. Wang, J. Clarke, S. Ja, D. Goad, L. Wald, E. Flood, E. Knobbe, J. Hryniewicz, S. Chu, D. Gill, W. Chen, O. King and B. E. Little, *Biosens. Bioelectron.*, 2008, **23**, 939–944.

17 L. Xu, W. Liang, Y. Wen, L. Wang, X. Yang, S. Re, N. Jia, X. Zuo and G. Liu, *Biosens. Bioelectron.*, 2018, **99**, 424–430.

18 C. R. Nemr, S. J. Smith, W. Liu, A. H. Mepham, R. M. Mohamadi, M. Labib and S. O. Kelley, *Anal. Chem.*, 2019, **91**, 2847–2853.

19 Y. Yang, Y.-Y. Yu, Y.-Z. Wang, C. L. Zhang, J. X. Wang, Z. Fang, H. Lv, J. J. Zhong and Y. C. Yong, *Biosens. Bioelectron.*, 2017, **98**, 338–344.

20 H. J. Sismaet, A. J. Pinto and E. D. Goluch, *Biosens. Bioelectron.*, 2017, **97**, 65–69.

21 H. Lee, J. O. Keem, H. Cho, J. M. Choi, W. S. Chung, D. Y. Jeon, D. S. Lee and Y. B. Shin, *Biosens. Bioelectron.*, 2018, **118**, 153–159.

22 A. Ahmed, J. V. Rushworth, N. A. Hirst and P. A. Millner, *Clin. Microbiol. Rev.*, 2014, **27**, 631–646.

23 F. Boulmedais, B. Frisch, O. Etienne, P. Lavalle, C. Picart, J. Ogier, J. C. Voegel, P. Schaaf and C. Egles, *Biomaterials*, 2004, **25**, 2003–2011.

24 J. Jin, Y. Han, C. Zhang, J. Liu, W. Jiang, J. Yin and H. Liang, *Colloids Surf., B*, 2015, **136**, 838–844.

25 K. D. Park, Y. S. Kim, D. K. Han, Y. H. Kim, E. H. B. Lee, H. Suh and K. S. Choi, Bacterial adhesion on PEG modified polyurethane surfaces, *Biomaterials*, 1998, **19**(7–9), 851–859.

26 Q. Wang, E. Uzunoglu, Y. Wu and M. Libera, *ACS Appl. Mater. Interfaces*, 2012, **4**, 2498–2506.

27 M. Zhang, T. Desai and M. Ferrari, *Biomaterials*, 1998, **19**, 953–960.

28 V. Hynninen, L. Vuori, M. Hannula, K. Tapio, K. Lahtonen, T. Isoniemi, E. Lehtonen, M. Hirsimäki, J. J. Toppari, M. Valden and V. P. Hytönen, *Sci. Rep.*, 2016, **6**, 29324.

29 A. B. González-Guerrero, J. Maldonado, S. Dante, D. Grajales and L. M. Lechuga, *J. Biophotonics*, 2017, **10**, 61–67.

30 S. Dante, D. Duval, D. Fariña, A. B. González-Guerrero and L. M. Lechuga, *Laser Photonics Rev.*, 2015, **9**, 248–255.

31 D. Grajales, A. Fernández-Gavela, C. Domínguez, J. R. Sendra and L. M. Lechuga, *J. Phys.: Photonics*, 2019, **1**, 025002.

32 J. Maldonado, A. B. González-Guerrero, C. Domínguez and L. M. Lechuga, *Biosens. Bioelectron.*, 2016, **85**, 310–316.

33 K. E. Zinoviev, A. B. Gonzalez-Guerrero, C. Dominguez and L. M. Lechuga, *J. Lightwave Technol.*, 2011, **29**, 1926–1930.

34 S. Lan, M. Veiseh and M. Zhang, *Biosens. Bioelectron.*, 2005, **20**, 1697–1708.

35 K. B. Roberts and E. R. Wald, *Pediatrics*, 2018, **141**, e20173239.

36 M. Woodhead, F. Blasi, S. Ewig, J. Garau, G. Huchon, M. Ieven, A. Ortqvist, T. Schaberg, A. Torres, G. van der Heijden, R. Read and T. J. Verheij, *Eur. Respir. J.*, 2005, **26**, 1138–1180.

37 K. Loens, L. Van Heirstraeten, S. Malhotra-Kumar, H. Goossens and M. Ieven, *J. Clin. Microbiol.*, 2009, **47**, 21–31.

38 O. Opota, A. Croxatto, G. Prodhom and G. Greub, *Clin. Microbiol. Infect.*, 2015, **21**, 313–322.

39 B. Blázquez, L. I. Llarrull, J. R. Luque-Ortega, C. Alfonso, B. Boggess and S. Mobashery, *Biochemistry*, 2014, **53**, 1548–1550.

40 T. K. McKinney, V. K. Sharma, W. A. Craig and G. L. Archer, *J. Bacteriol.*, 2001, **183**, 6862–6868.

41 J. H. Kwon, M. K. Fausone, H. Du, A. Robicsek and L. R. Peterson, *Am. J. Clin. Pathol.*, 2012, **137**, 778–784.

42 E. J. G. Pollitt, P. T. Szkuta, N. Burns and S. J. Foster, *PLoS Pathog.*, 2018, **14**, e1007112.

